JOURNAL OF MATERIALS SCIENCE: MATERIALS IN MEDICINE **17** (2006) 81–94

Zinc phosphate as versatile material for potential biomedical applications Part 1

L. HERSCHKE, J. ROTTSTEGGE, I. LIEBERWIRTH*, G. WEGNER
Max Planck Institute for Polymer Research, Ackermannweg 10, D-55128 Mainz, Germany
E-mail: lieberw@mpip-mainz.mpg.de

Synthetic α- and β-Hopeite, two polymorphs of zinc phosphate tetrahydrates (ZPT) have been synthesized by hydrothermal crystallization from aqueous solution at 20 °C and 90 °C respectively. Aside from their subtitle crystallographic differences originating from a unique hydrogen bonding pattern, their thermodynamic interrelation has been thoroughfully investigated by means of X-Ray diffraction (XRD) and differential scanning calorimetry (DSC), combined with thermogravimetry (TGA-MS). Using a new heterogeneous step-reaction approach, the kinetics of dehydration of the two forms of ZPT was studied and their corresponding transition temperature determined. Low temperature DRIFT, FT-Raman and ^{1}H, ^{31}P MAS-NMR reveal an oriented distortion of the zinc phosphate tetrahedra, due to a characteristic hydrogen bonding pattern and in accordance with the molecular tetrahedral linkage scheme of the phosphate groups. Biogenic Hydroxyapatite (HAP) and one of its metastable precursors, a calcium dihydrogen phosphate dihydrate (DCPD) or Brushite were also obtained and used to underline the resulting variations of chemical reactivity in zinc phosphates.

Introduction

Materials research devoted to the development of new or improved hybrid materials based on metal phosphate hydrate cements with enhanced mechanical and chemical stability, suitable partial or permanent restoration of bone and teeth attracts much interest at the interface between medicine, inorganic and physical chemistry and ceramic science.

In particular self-setting Hydroxyapatite [$Ca_5(PO_4)_3(OH)$] (HA) bone cements have received significant attention since the 1980s due to their similarity with natural bone minerals [1, 2]. Despite favourable biocompatiblity [3, 4], the brittle nature of HA cements yield inferior strength when compared to natural bone [5–8]. The increased use of HA cements in orthopaedic applications provides compelling motivation for an improved understanding of the underlying structures and mechanisms that govern the useful properties of these materials [9].

Similarly, zinc phosphate [$Zn_3(PO_4)_2 \cdot x H_2O$] (thereafter ZP) cements have been used in dentistry for many years and as early as 1879 as joint material between tooth root and crown [10]. Recent research was devoted to the setting process and to changes in solubility as setting proceeds in physiological conditions [11–13]. It is now known that the initial product formed is a soluble acidic zinc phosphate, that rapidly undergoes further reaction, resulting in steadily decreasing solubility. This has been attributed to the formation of amorphous zinc orthophosphate $Zn_3(PO_4)_2$ [14–16], a substance that is sparingly soluble in water. However, over long periods of time, some material does crystallize, forming its hydrated phase [$Zn_3(PO_4)_2 \cdot 4\ H_2O$] known as Hopeite [17]. Hopeite formation ensures low solubility, good adhesion, excellent durability and biocompatibility of dental cements [18–21]. In nature zinc phosphate tetrahydrate exists in two structures, orthorhombic Hopeite and ParaHopeite, its triclinic polymorph [22, 23]. Although the phase system P_2O_5-ZnO-H_2O was studied for a very long time [24, 25], the precise structure of the two orthorhombic modifications, α- and β-Hopeite, was not precisely known [26, 27]. In a previous study, we have reported on the preparation of the two polymorphs of zinc phosphate tetrahydrate in comparison with ZP impure forms and on their crystal structure [28]. It was shown that α- and β-Hopeite differ with regard to their hydrogen bonding network; the α-form has a three dimensional H-bond connectivity while

*Author to whom all correspondence should be addressed.

the β-form exhibits a two dimensional bond connectivity, preferentially oriented along the *b*-axis. Albeit their crystal structure is now fully determined, the intrinsic properties of the pure polymorphs remain yet essentially unknown [29, 30].

Synthetic HA and ZP precursors can be produced by a variety of ceramics processing routes including precipitation, electrophoretic deposition, sol-gel reaction, hydrothermal processing, pyrosol method, pulsed laser–plasma spraying as first summarized by Akao *et al*. and then by Dorozhkin *et al*. [31–37]. The cement aging in both types of materials involves exchange of anions (phosphate, fluoride, hydroxide, carbonate) [38–41] and numerous changes in the hydration state [42, 43] leading to complex but nearly identical formulations [44] with chemically similar intermediary products such as α-$Ca_3(PO_4)_2$ (vs α-$Zn_3(PO_4)_2$) [45, 46]. In addition, calcium and zinc being both octahedrally coordinated, It is possible to exchange calcium with zinc ions [47–51]. Hence, zinc has shown dramatic influence in delaying or modifying the crystallization process of Hydroxyapatite, as zinc hydrogen phosphate $Zn(HPO_4)_2{\cdot}3H_2O$, Hopeite $Zn_3(PO_4)_2{\cdot}4H_2O$, Scholzite $CaZn(PO_4)_2{\cdot}2H_2O$ and Whitlockite β-$Ca_3(PO_4)_2$ (β-TCP) form all in an incomplete reaction due to local fluctuations of temperature or pH [52–55]. Therefore, an investigation of a simpler system like the zinc phosphate tetrahydrate alone, is the rational approach to gain clear information about the more complex apatite/Hydroxyapatite system.

We are not aware of any studies that concentrates on a basic analysis of the structure-properties relations of such metal phosphates needed not only to understand the mechanical properties of synthetic apatite/Hydroxyapatite bone cements but also the chemical stability and solubility of zinc phosphate dental cements.

In the present study, the primary interest is, apart of the differentiation of the zinc phosphate tetrahydrates (α- and β-Hopeite) in direct relation with their crystal structure, careful analysis of their thermal stability. Further the evaluation of the chemical stability and surface reactivity of ZP polymorphs, in comparison with Hydroxyapatite is expected to provide basic information about the possible polymer-crystal surface interactions and beyond, to offer a starting point for future efficient modifications of Hydroxyapatite based materials such as bone replacement cements [56]. This goal benefits from the assumption that pure Hopeite can be used as model.

Experimental

Synthesis of α-,β-zinc phosphate tetrahydrate (ZPT) crystalline powders

Large crystals of zinc phosphate tetrahydrates were obtained by mixing 100 mL of 0.114 mol $\cdot$ L^{-1} zinc acetate (Aldrich, ACS grade) solution with 5.5 mL of a four times diluted phosphoric acid solution (Aldrich, ACS grade, 85 wt% solution) in order to achieve the following molar ratio $Zn{:}PO_4 = 1{:}1.05$, during at least two hours at pH 4 and mild stirring at 90.0 °C and 20.0 °C for α- and β-ZPT, respectively. Important factors are the control of the crystallization temperature, which was achieved using a thermostated double-walled crystallization reactor with a precision of 0.1 °C, the mechanical stirring rate of 500 rpm, and the pH of the reaction medium, which was fixed in adding alternatively aliquots of a 4 mol $\cdot$ L^{-1} NaOH solution (NaOH pellets, Riedel-de-Haën, ACS grade) and of a 4 mol $\cdot$ L^{-1} HNO_3 solution. At the start of the reaction a white precipitate forms and redissolves quickly as the pH reaches 1.45 while stirring at 1250 rpm. The pH is then rapidly adjusted to 4. The reaction was kept inert gas atmosphere (argon) and evaporation of water was prevented. Crystalline product was recovered from the mother liquor by filtration and washed to neutral pH to eliminate traces of adsorbed hydrogen phosphate and dried at room temperature for 12 h. Deuterated samples were obtained using corresponding amounts of D_2O (Deutero GmbH, spectroscopic grade) instead of Millipore grade water.

Brushite and hydroxyapatite (HAP)

A 0.375 mol $\cdot$ L^{-1} orthophosphoric acid solution was added at a drop rate of 1-2 drops/s to a solution of 0.5 mol $\cdot$ L^{-1} calcium acetate dihydrate (Fluka) to form a gelatinous precipitate at a temperature of 40 $\pm$ 0.1 °C. The pH value of 7.5 was controlled by addition of necessary amounts of tetramethylammonium hydroxide (25 wt% solution in water) and 4 mol $\cdot$ L^{-1} NaOH solution during the crystallization. The precipitate was left in the mother solution overnight and the supernatant was decanted. After washing the precipitate, it was centrifuged (4000 rpm, Hettich Laboratory centrifuge ROTIXA 120 R) and oven-dried at 65 °C in vacuo overnight. Using the same process, stoichiometric HAP crystals were prepared by keeping the above-mentioned reactants at pH 11. Dichloromethane was added and the nanocrystals were recovered by decantation of the mother liquor. The crystalline precipitate was washed twice with Millipore-grade water, followed by centrifugation at 16000 rmp (Beckman L8.M Ultracentrifuge) and dried at 65 °C for 12 h.

Characterization

Elemental analysis of the precipitate was conducted by atomic absorption spectroscopy (Perkin Elmer PE 5100 ZL with Zeeman Furnace Module and AS 70 sampler) and by colorimetric phosphate titration (blue molybdate complexometric method) using UV/Vis spectrometry (PE Lambda 900) [46]. pH values were measured with a Pt/KCl glass electrode attached to a pH meter (Schott CG 843 set) with integrated temperature sensor

(Blueline 14 pH, Schott). Prior to the measurements, the pH electrode was calibrated using 3 buffer solutions at pH = 4.006, 6.865, 9.180 at 20.0 °C (DIN Norm 19266). DSC measurements were performed under nitrogen on a Mettler-Toledo DSC 30S module with a TC15 TA controller. (heating rate: 10 °C · min^{-1}, heating range: 0–500 °C) Similarly TGA-MS curves were obtained under argon on a Mettler-Toledo ThermoSTAR^e TGA/SDTA 851 equipped with a Pfeiffer Vacuum GSD 300 T2 pump and a Balser MS/Netsch STA449C mass detector (heating rate: 10 °C·min^{-1}, heating range 0 to 600 °C).

DRIFT spectra (Diffuse Reflectance Infrared Fourier Transform) were recorded with a Nicolet 730 spectrometer (liquid N_2 cooled MCT detector) on powder samples (10 wt% sample, 90 wt% KBr, total amount 300 mg). Spectra were collected with a nominal resolution of 4 cm^{-1}, double averaging over 128 scans in the frequency range 400–4000 cm^{-1}. Low temperature data were collected using a variable temperature cell (Graseby Specac) driven by a Eurotherm controller 808. FT-Raman spectra in the region 3500–100 cm^{-1} were obtained on a Brucker RFS 100/s Fourier Transform spectrometer (resolution 1 cm^{-1}) equipped with a Nd^{3+}:YAG laser (excitation wavelength: 1064 nm) and a liquid nitrogen cooled Ge detector. Samples were measured using KBr disks (5 wt%) in by backscattering geometry. The laser output was 100 mW to minimize fluorescence of HAP, and 2000 scans were collected on average. Precise peak position were determined by second derivative local minima analysis.

Powder X-ray data for an as-synthesised sample of crystals (placed on 2 cm circular silicium monocrystal slide) were collected at 25 °C on a SEIFERT XRD 3000 TT Bragg-Brentano diffractometer with a linear position sensitive detector (5 ° 2θ) in Debye-Soller geometry with a flat secondary monochromator and employing Ge monochromated Cu Kα_1 radiation (λ = 1.5406 Å) and also equipped with a MRI TC-radiation heating chamber (heating rate: 10 °C/min, heating range: 25–600 °C).

Solid State Nuclear Magnetic Resonance (NMR) spectra were acquired at a BRUKER DSX 500 spectrometer operating at a magnetic field of 11.74 T. All ^{1}H and ^{31}P MAS-NMR spectra were measured using 2.5 and 4mm rotors with commercial double resonance probes and spinning speeds of 10 to 25 kHz as described elsewhere [57, 58]. The 90 ° pulse length was 3 μs for the ^{1}H measurements and 4 μs for the ^{31}P measurements. The recycle delay was 3 seconds (^{1}H spectra) and 20 seconds (^{31}P spectra).

Results and discussion

Differentiation between α- and β-Hopeite, and α-, β-zinc phosphate dihydrate

The crystal structure of the zinc phosphate polymorphs, α- and β-Hopeite differ by the hydrogen bonding pattern, leading to characteristic differences in thermal behaviour. In agreement with extensive characterizations conducted first by Yaglov and Volkov [59, 60] and more recently by Gardner and McAra [26], it must be concluded that the α-Hopeite is the most stable phase and possesses a higher activation energy of dehydration than β-Hopeite.

The studies of zinc phosphate hydrates has so far suffered from a lack of accuracy and the contradictory information on the dehydration processes of the pure Hopeite polymorph. This gave reason to carry out a detailed study of the dehydration of structurally pure α- and β-Hopeite. Fig. 1 displays the successive dehydration steps of α-Hopeite (Fig. 1(a)) and β-Hopeite (Fig. 1(b)) at 220 °C and 600 °C in terms of XRD. The starting materials were chemically pure and their measured powder diffractograms correspond very well with the simulated powder diffractograms (MSI, Cerius 2 (2001)) using the previouly determined crystallographic data for each phase [28]. The stochiometric composition was calculated as follows within the limits of analytical error (elemental analysis and thermogravimetry): α-Hopeite: $Zn_3(PO_4)_2{\cdot}4H_2O$, β-Hopeite: $Zn_3(PO_4)_2{\cdot}4H_2O$, Brushite: $Ca_1(HPO_4)_1{\cdot}2H_2O$ and Hydroxyapatite $Ca_5(PO_4)_3(OH)$. In the case of α- and β-Hopeite,these values match nearly perfectly with the zinc phosphate tetrahydrate stoichiometry. Thanks to preliminary DSC experiments, one may conclude that the zinc phosphate dihydrate exist between 200 and 240 °C, and that the anhydrate is stable above 600 °C until 650 °C without occurrence of reversible metamorphism, as it was duly noted by Calvo [61]. The diffractograms obtained at 200 °C and above do not correspond to known intermediary structures such as zinc phosphate trihydrate or monohydrate [62] and are not exactly identical to earlier published results of Gérault *et al*. about zinc phosphate dihydrate [63, 64]. At 600 °C, the XRD data are similar to those of α-,β-$Zn_3(PO_4)_2$ [65].

Kotlova *et al*. [66] have prepared a dihydrate polymorph and have characterized it by XRD and thermal analysis. They designated this polymorph as "active" form or β-dihydrate in that it behaves more hygroscopically than the "normal" dihydrate, also called α-zinc phosphate dihydrate, and abusively α-dihydrate. They affirmed that this β-form, also produced by McAra [26] in another way (room temperature and reduced pressure), converts into the α-dihydrate at approximatively 150 °C until 200 °C at ambient pressure. In contradiction to these results, our XRD studies confirm that there is no spontaneous transformation from the β-dihydrate to the α-dihydrate. α- and β-zinc phosphate dihydrates possess different powder diffractograms, thus indicating different crystal structures, and the kinetics of the thermal dehydration discussed later in this study speak against such an assumption. In addition, Arnaud *et al*. [67] determined the structure of the α-dihydrate from powder diffractogram. However, the crystal structure of

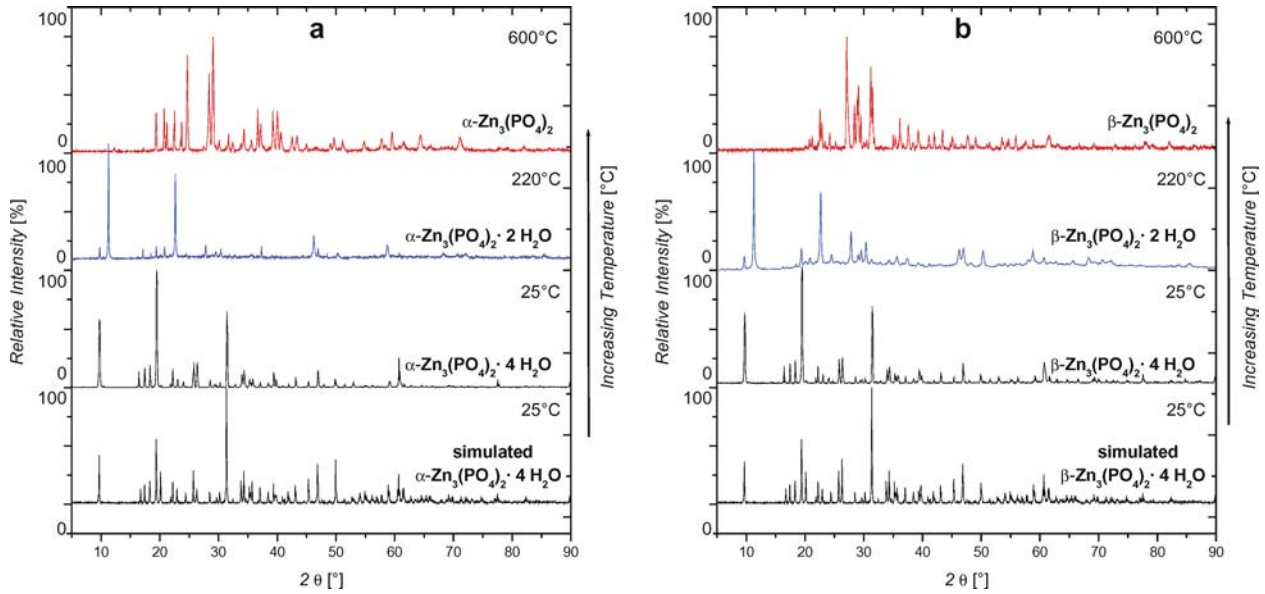

Figure 1 X-ray powder pattern of: (a) α-Hopeite; (b) β-Hopeite, at various temperatures corresponding to their respective hydrated phases. At room temperature, comparison between experimental and simulated spectra.

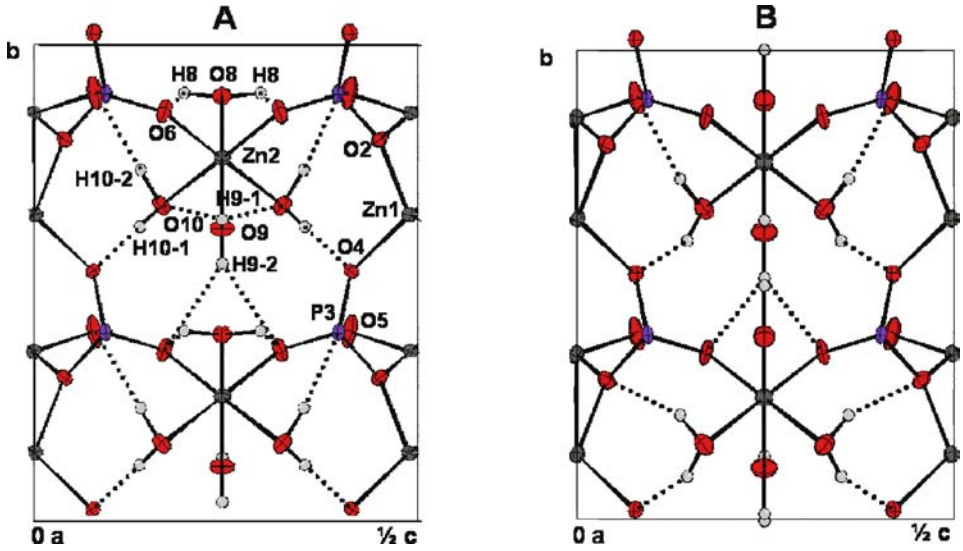

Figure 2 Composition of a half asymmetric unit cell of (A) α-Hopeite and (B) β-Hopeite projected along the a-axis. The same nomenclature is used for β-Hopeite. Dash lines represent hydrogen bonds.

β-dihydrate has not been yet determined. During dehydration from tetrahydrate to dihydrate, the alteration of the structure occurs in planes parallel to $(001)_{dh}$ of the dihydrate which corresponds to $(010)_{hop}$. Justified by the fact that the **a** and **b** cell parameters remain practically unchanged during dehydration, the structural contraction occurs only in the $(010)_{hop}$ plane within the PO_4^{3-}-Zn(1)-PO_4^{3-} sequence (Fig. 2). In consequence, the Zn(1)-type zinc atoms [68] undergo a change of coordination from octahedric to tetrahedric during dehydration, and this configuration is stabilized by hydrogen bonding along the $(001)_{dh}$-axis. Therefore, in analogy to the structural difference between α- and β-Hopeite, the crystallographic difference between α- and β- zinc phosphate dihydrates may lie similarly in the hydrogen bonding pattern. Using DSC and TGA-MS experiments as follows, this conclusion will be confirmed.

Thermal stability of zinc and calcium phosphates hydrates

Both orthorhombic modifications of $Zn_3(PO_4)_2{\cdot}4\ H_2O$ show dehydration starting above 100 °C. It appears to be complete at about 400 °C as shown by DSC and TGA-MS in Figs. 3 and 4. At higher temperatures, decomposition or "condensation" of phosphate groups in

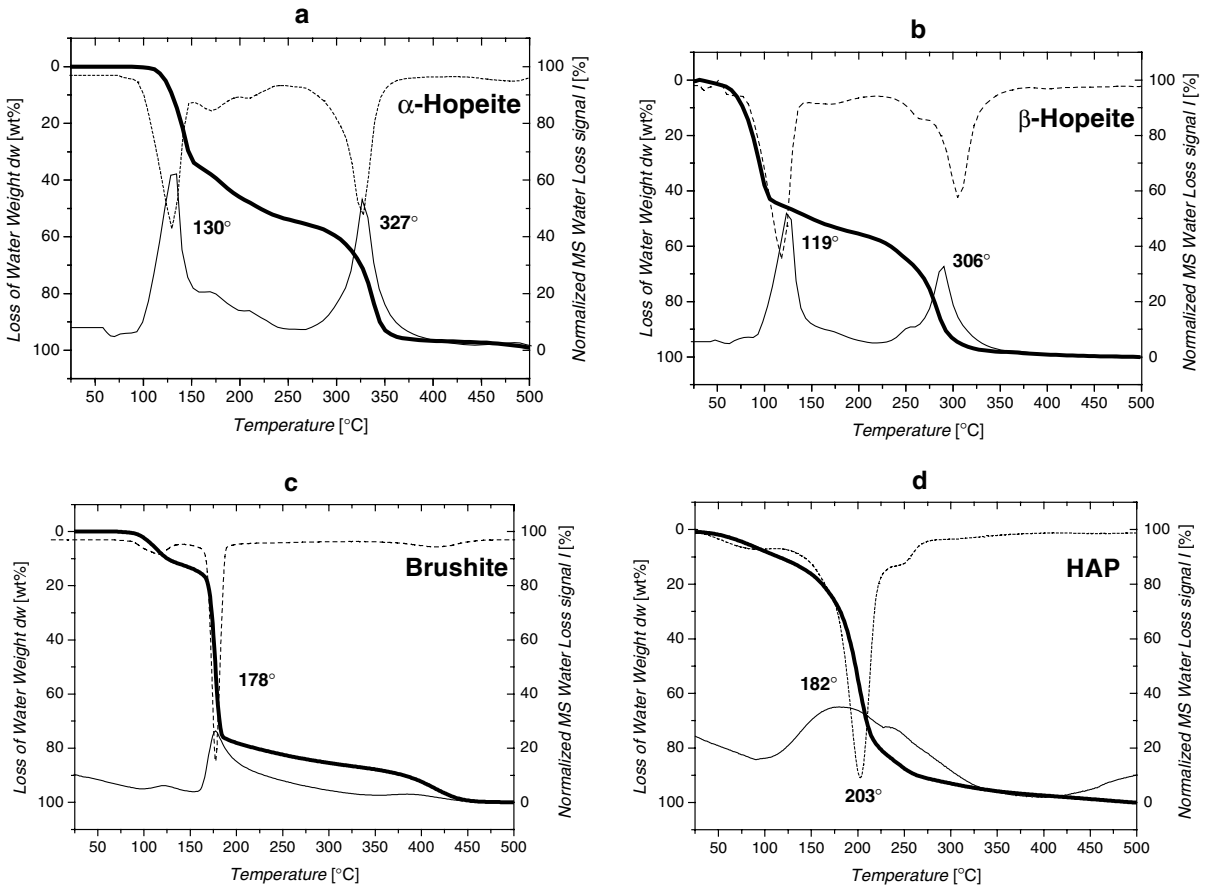

Figure 3 Comparison of TGA-MS thermograms of (a) α-Hopeite, (b) β-Hopeite, (c) Brushite, (d) Hydroxyapatite taken at 10 K·min^{-1}. Loss Weight (thick line), First order derivate (dash line) of the loss weight curves and MS water signal (m/s:18, dark line) are given as normalized to 100%. This corresponds to the loss of four water molecules for the Hopeite samples. Similarly, it describes the loss of one and two water molecules for HAP and Brushite samples.

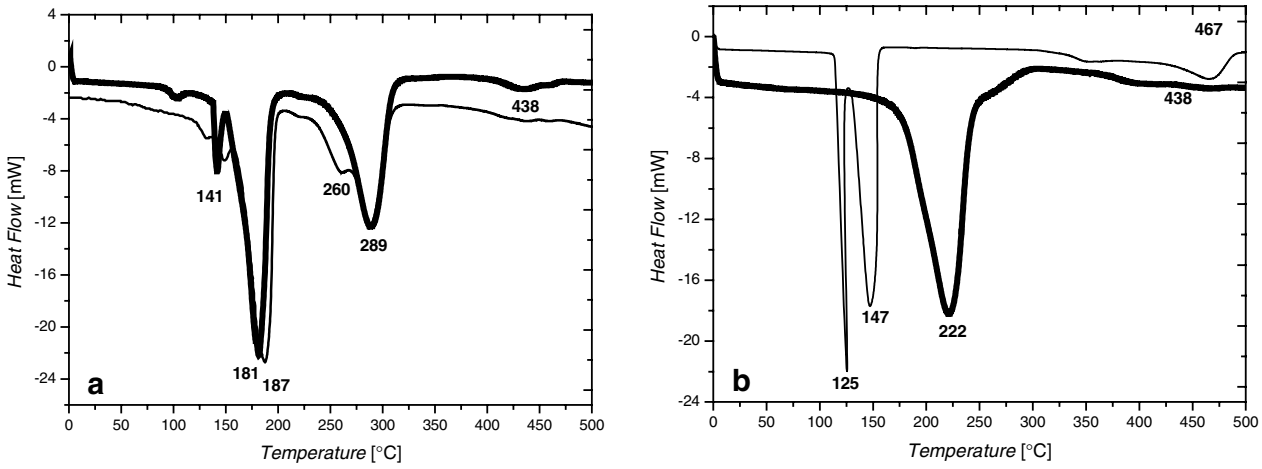

Figure 4 Comparison of DSC curves taken at a heating rate of 10 K·min^{-1} of (a) α-,β-Hopeite and of (b) Brushite and HAP. While α-Hopeite and HAP are described with thick black lines, β-Hopeite and Brushite are shown in thin line. Peak temperatures measured are also given.

pyrophosphate groups are expected [73]. From Fig. 4(a), this takes places at 438 °C for the Hopeite polymorphs [69]. As well, hydrogen phosphate groups belonging to a Brushite crystal structure may similarly "condense" above 467 °C into calcium pyrophosphate ($Ca_2P_2O_7$). The thermogravimetric curves (Fig. 3) show that α-Hopeite loses crystal water in two well defined steps: two molecules at 130 °C and the remaining two at

327 °C. Similarly DSC (Fig. 4) gives two well separated peaks but slightly displaced: one sharp peak at 182 °C and another one at 289 °C which indicates the starting point for the loss of two types of water molecules. At about 220 °C, i.e. after loss of $2H_2O$, a pseudo-stabilization of the structure is reached; the water loss is much reduced, indicating the existence of a dihydrate structure. In the light of these results, one can confirm that the first step corresponds to the transition Tetrahydrate-Dihydrate while the second step to the transition Dihydrate-Anhydrate [67, 70].

The thermograms of β-Hopeite show significant differences compared to the α-form. β-Hopeite seems to be less stable with regard to dehydration pointing toward a lower symmetry of the four water molecules contained in the crystal structure. This is confirmed by DSC where the onset point of the thermal decomposition appears at 115 °C for the β-form compared to 130 °C for the α-form (Fig. 4(a)). A four-step dehydration starts with the loss of one water molecule, corresponding to an unstable trihydrate intermediary structure at 141 °C, rapidly followed by the loss of a second water molecule (removal of 1.96 H_2O), marked by a broad endothermic peak at 181 °C. While no graduation is clearly observable on the TGA-weight loss curve of β-Hopeite between the dihydrate and the anhydrous salt, the DSC curve presents two peaks at 260 and 289 °C, and one can see a shoulder on the TGA-curve at a water content corresponding to the monohydrate [63]. Surprisingly, the weak transition at 238 °C may indicate a conformational rearrangement of the β-dihydrate since no water is lost at that temperature, which corresponds also to the temperature where the dihydrate starting from α-$Zn_3(PO_4)_2{\cdot}4\ H_2O$ is well formed [71]. In conclusion, the β-HHopeite looses its four water molecules one after another in four consecutive steps. These results are in partial disagreement with the thermal behaviour of β-Hopeite previously reported in the literature [72].

Similarly to β-Hopeite, Brushite loses its two crystal water molecules successively at 125 and 147 °C (DSC, Fig. 4(b)), as indicated by a broad water peak in the TGA-MS thermogram (Fig. 3(c)) [73a] and finally transforms into calcium hydrogen phosphate anhydrate (i.e. DCPA, monetite) above 220 °C [73b,c]. Furthermore, the weight loss curve shows a drastic change and its first derivative displays a sharp peak at 178 °C, suggesting that the two crystal waters of Brushite are not energetically equivalent. Hydroxyapatite shows a single well-defined but very broad dehydration peak with onset around 175 °C and peak maximum at 222 °C by DSC (Fig. 4(b)), corresponding to a dehydroxylation followed by a decomposition/collapse of the HAP structure into other forms of calcium phosphates such as tricalcium phosphate or tetracalcium phosphate [74a,b]. This corresponds to a broad water release detected in TGA-MS with a maximum around 182 °C (Fig. 3(d)).

These marked differences in thermal behaviour observed for α-,β-Hopeite on one side and for Brushite/HAP on the other side should be correlated either to crystallographic and thermodynamic differences relative to the hydrogen bonding pattern, or to purely kinetic effects. In order to elucidate this, a thermodynamic-kinetic study focused on the dehydration reaction of α- and β-Hopeite was conducted.

Thermodynamic stability and dehydration kinetics of α- and β-Hopeite.

The standard enthalpies ($\Delta H^{\text{dehydr.}}$), entropies ($\Delta S^{\text{dehydr.}}$) and free energies ($\Delta G^{\text{dehydr.}}$) of dehydration of the zinc phosphate hydrates, depending on their crystallographic phase, have been generated from DSC measurements in averaging over 8 runs at linear increasing heating rates [0.5, 1, 2, 5, 10, 15, 20 $\text{K} \cdot \text{min}^{-1}$].

The values of ΔH and ΔG obtained from DSC are similar to the solubilisation enthalpies obtained for by McAra *et al.* [27] for a rehydration from $Zn_3(PO_4)_2{\cdot}2H_2O_{(l)}$ to $Zn_3(PO_4)_2{\cdot}4H_2O_{(\text{cr})}$. Surprinsingly, by selective dissolution reaction calorimetry, Yaglov [75, 76] and then Volkov [77, 78] obtained separately a set of thermodynamical data for α-,β-Hopeite (α-,β-ZPT or α-,β-tetrahydrate) that vary as much as 25% with our measured $\Delta H^{\text{dehydr.}}$ values, especially concerning the dihydrate state (α-,β-ZPD or α-,β-dihydrate) (Table I). This is certainly due to impurities contained in the starting material (zinc oxide, zinc hydrogen phosphate). It could also originate from the "same final thermodynamic state" procedure, described as a solid-liquid reaction, while the present method considers a solid-gas reaction ($\Delta H^{\circ}_{\text{form.}}(H_2O) = -241.8\ \text{kJ} \cdot \text{mol}^{-1}$, $S^{\circ}_{\text{form}}\ (H_2O) = -228.6\ \text{J} \cdot \text{mol}^{-1} \cdot \text{K}^{-1}$) [79–81].

The direct comparison of the relative thermodynamic stabilities of α- and β-Hopeite is here of interest. As a strong parallel, α- and β-$Ca_3(PO_4)_2$ (α,β-TCP) originating from the dehydration of Hydroxyapatite [82–84] have not only nearly identical free energy as α,β-Hopeite ($-4120/-4110$ in comparison with $-4100/-4090\ \text{kJ} \cdot \text{mol}^{-1}$) [85], but also possess similar entropy ($0.249/0.236\ \text{kJ} \cdot \text{mol}^{-1} \cdot \text{K}^{-1}$ for α-,β-TCP). Further assuming that one obtains the same anhydrate state from α- and β-Hopeite the data in Table II indicate a the stability difference for the α-, β-form of dihydrate and tetrahydrate of 6.1 and $31.1\ \text{kJ} \cdot \text{mol}^{-1}$ respectively. These values are significantly higher than the experimental error and once again in good agreement with the estimates of McAra *et al.* These authors obtained 4.1 and $5.4\ \text{kJ} \cdot \text{mol}^{-1}$ respectively. Finally, a comparison of this set of data with the numerous values published in the literature [86–89] seems to point out that particle size effects need to be considered. The small size of the crystals which are commonly investigated leads

TABLE I Extrapolated thermodynamic values of dehydration process from DSC curves at a heating rate β of zero K·min^{-1} given at transition temperature for the two zinc phosphate tetrahydrate polymorphs

Hydration state of crystals	Transition temp. T_{max}(°C)	$\Delta H^{dehydr.c}$ (kJ/mol)	$\Delta H^{dehydr.c}_{Lit}$ (kJ/mol)	$\Delta S^{dehydr.c}$ (kJ/mol·K)	$\Delta G^{dehydr.d}$ (kJ/mol)	$\Delta G^{dehydr.}_{Lit}$ (kJ/mol)
α-dihydrate[a]	174.7	−111	−102[e]	−0.33	36	30
α-anhydrate	266.1	−75	−125[e]	−0.20	32	29
β-dihydrate [b]	184.6	−105	−94[f]	−0.30	30	29
β-anhydrate	277.5	−75	−120[f]	−0.19	27	27

[(a)]mass of zinc phosphate tetrahydrate in vacuo: 458.11 g·mol^{-1}.
[(b)]mass of zinc phosphate dihydrate in vacuo : 422.11 g·mol^{-1}.
[(c)]estimed errors $T \pm 0.1$°C, $\Delta H \pm$ 0.5 kJ·mol^{-1}.
[(d)] ΔG calculated at transition temperature, experimental error ±1.0 kJ·mol^{-1}.
[(e)]from Ref. [63, 71].
[(f)]from Ref. [67, 70].

TABLE II Standard thermodynamic values of formation of zinc orthophosphates and its hydrates, calculated form dehydration reaction at 25 °C

Hydration state of crystals	$\Delta H^{\circ}_{form.}$ (kJ·mol^{-1})*	$\Delta H^{\circ}_{formLit}$ (kJ · mol $^{-1}$)*	ΔG°_{form} (kJ · mol $^{-1}$)*	$\Delta G^{\circ}_{formLit}$ (kJ · mol^{-1})*	$S^{\circ}{}_{form}$ (J · mol^{-1} · K^{-1})*
α-tetrahydrate	−4086	−4093[a]	−3613	−3628[f]	253
β-tetrahydrate	−4055	−4091[c]	−3605	−3616[f]	291
α-dihydrate	−3486	−3492[a]	−3126	–	451
β-dihydrate	−3480	−3487[a]	−3120	–	477
anhydrate	−2891[b]	−2891[d]	–	−2633[e]	779[g]

[(a)]from Ref. [26].
[(b)]recalculated from ref. 21 using ΔH^{c}_{form}[ZnO,c] = - 350.4 kJ · mol^{-1} and $\Delta H^{c}_{form}[PO_4^{3-}$,liq.] = −1277.4 kJ·mol^{-1}
[(c)]from Ref. [87].
[(d)]from Ref. [69].
[(e)]from Ref. [67].
[(f)]from Ref. [88].
[(g)]recalculated from ref. [87] for a ionic crystal using $S^{\circ}{}_{form}[Zn^{2+}]$ = 153.8 J · mol^{-1} · K^{-1} and $S^{\circ}{}_{form}[PO_4^{3-}]$ = 159.0 J · mol^{-1} · K^{-1}
(*)estimed errors T ± 0.1 °C °C, $\Delta H \pm$ 0.5 kJ · mol^{-1}, $\Delta G \pm$ 1.0 kJ · mol^{-1} and S° ± 4 J · mol^{-1} · K^{-1}

to a strong contribution of surface energy to the overall thermodynamic stability of the material. Therefore data from other authors may differ from our set of data. The present method describes dehydration in the crystalline state (in contact with argon) and the one of I.W. McAra *et al*. for the rehydration of a crystal immersed in a concentrated H_3PO_4 solution or in liquid water. Crystals of α- and β-Hopeite are nearly of same size (micron domain), so it is possible to neglect surface effects and to compare directly the obtained thermodynamic data. In Table II, the marked differences of absolute entropy of formation for the α- and β-forms of zinc phosphate tetrahydrates/dihydrates firstly prove that the α-form is more stable than the β-form, due to the lower entropy of the α-form.

On the basis of the close connection between thermal stability and hydrogen bond strength, one may conclude that the evaluation of the "activation energy of dehydration" should be a direct measure of the hydrogen bond strength, thus confirming the crystallographic and thermodynamic interrelation of α- and β-zinc phosphate tetrahydrates [90].

The α-Hopeite possesses a three dimensional hydrogen bond network stabilizing the structural units while the β-Hopeite has only a two dimensional hydrogen bonding pattern. So, on heating the structure of α-Hopeite is destabilized in such a way that it transforms itself automatically to a dihydrate and to an anhydrate at higher temperature. The isothermal transition from the "metastable" β-form of ZPT to the most stable form α, is thermodynamically possible but kinetically not favoured. Results of Tables I and II suggest that α-ZPT can only dehydrates in the α-ZPD (i.e. β-ZPT $\rightarrow$ β-ZPD). To understand this dehydration mechanism clearly, a description with an intermediary state is necessary (Scheme 1). This is precisely illustrated by the fact that albeit submitting β-Hopeite crystals to water pressure at 90 °C for one year, no crystallographic changes to α-Hopeite occurs. Therefore the free energy of the β-ZPT$\rightarrow$ α-ZPT isothermal reaction (at 90 °C, synthesis temperature of α-Hopeite) and the thermal activation energy of the reaction β-ZPT$\rightarrow$ β-ZPD might be nearly identical at a *critical* temperature $T^{\neq}{}^{\circ}$ above 90 °C and under 220 °C, the stability temperature of

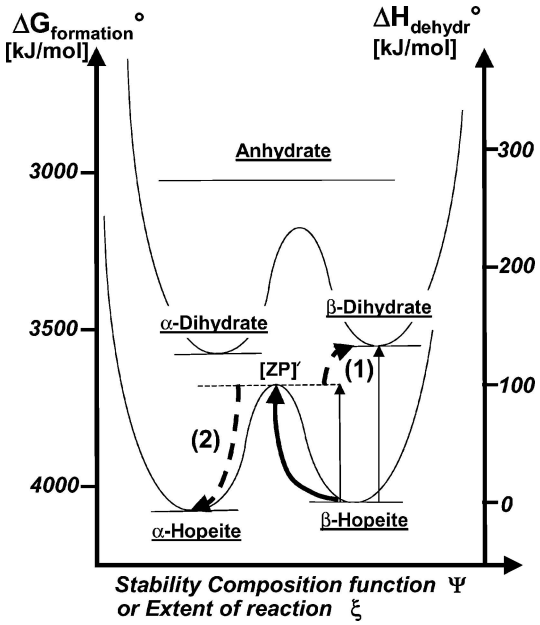

Scheme 1 Representation of the thermodynamic-kinetic interrelations between the different zinc phosphate anhydrate, dihydrate and tetrahydrate. From Hess law cycles, the stability difference ($\Delta G^\circ_{\text{formation}}$.) between α- and β-tetrahydrates and between α- and β-dihydrates are 8.7 and 6.5 kJ/mol respectively. Upon heating, the β-tetrahydrate is destabilized and two pathways are possible: A kinetic pathway (1) and a thermodynamic pathway (2).

β-zinc phosphate dihydrate, determined by DSC [91]. The extension to a null heating rate of the maximum dehydration rate versus heating rate directly converges logarithmically to a critical value $T^{\neq\,\circ}$(β-ZPT$\rightarrow$ α-ZPT) of 168.5 °C [92]. At that precise temperature, an isothermal conversion of β-Hopeite into α-Hopeite is not only thermodynamically possible but also kinetically favoured.

Vibrational analysis and structural stability

Besides analytical techniques, especially infrared, Raman and solid state NMR spectroscopy are excellently suited to characterize zinc phosphate [93–97]. Vibrational spectra also give important information about the structural changes that take place in Hopeite crystals upon heating, in presence of impurities or surface reactions.

For instance, DRIFT combined with FT-Raman allows a sensitive and fast detection of the two forms of zinc phosphate tetrahydrate. The symmetry of a "free" PO_4^{3-} ion is T_d and the nine modes of internal vibrations span the irreducible representation $\Gamma_{\text{vibr}}(T_d) = A_1 + E + 2F_2$ [98–99]. Here A_1 represents the symmetric stretching mode ν_s (P–O), located at ≈980 cm^{-1}. E represents the symmetric bending mode δ_s (OPO) at ≈420 cm^{-1}, and the triply degenerated modes F_2 represent the antisymmetric bending mode δ_{as} (OPO), located at ≈560 cm^{-1}. However slight shifts in the known spectra of α-, β-Hopeite have to be noticed due to solid-state effects and specificities of DRIFT technique [100]. Moreover, the 300 vibration modes of the unit cell of Hopeite decompose in 150 only Raman active modes and 111 IR active only modes. Since the crystal structure of both α- and β-Hopeite are centrosymmetric, the Raman modes display g-symmetry and their IR counterparts u-symmetry (mutual exclusion principle). The PO_4^{3-} ions contribute 27 IR and 36 Raman modes to the 106 active internal vibrations. The diverse kinds of hydrate water molecules give rise to 19 IR and 24 Raman modes.

Crystal water and hydrogen bonding

In hydrated solids, the translation and rotation modes of the crystal water molecules become frustrated and thus give rise to external H_2O librations and translational modes (lattice vibrations) in addition to internal stretching and bending vibrations. The librations usually give rise to bands in the range 900–300 cm^{-1}, and the translational modes appear between 350 and 100 cm^{-1} [101]. In ionic crystals, where the H_2O molecules are strongly involved in hydrogen bonding, the stretching modes are generally redshifted and hence can be usually observed in the range 3000–3600 cm^{-1}. It is well established that the H_2O bending modes are less sensitive to site symmetry effects and distorsions are observed in the range 1560–1660 cm^{-1}. For studying the local distortional geometry and evaluating the bond strengths of H_2O molecules, the DRIFT spectra of isotopically diluted samples (0, 25, 50 and 75% D) recorded at low temperature (90 K) and room temperature (Fig. 5, 25%

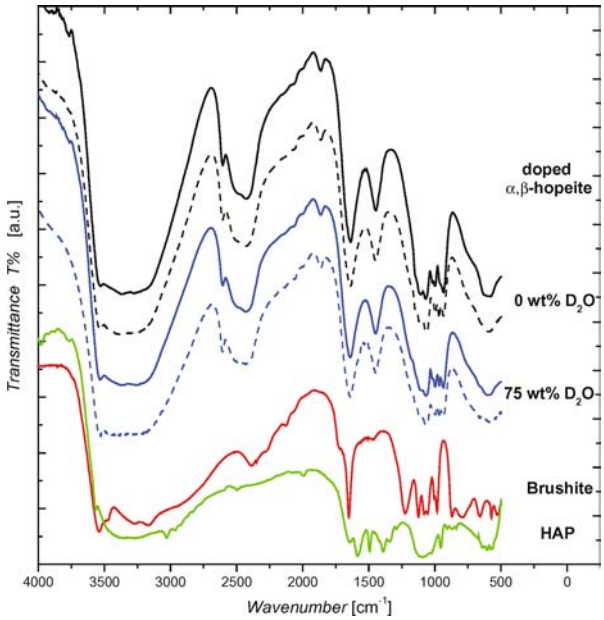

Figure 5 FTIR reflection spectra of orthorhombic α-Hopeite [full line], β-Hopeite [dash line], doped with increasing concentrations of D_2O at 25 °C. Comparison with monoclinic Brushite ($CaHPO_4 \cdot 2H_2O$) [black line] and hexagonal Hydroxyapatite ($Ca_5(PO_4)_3(OH)$) [red line].

and 50% not shown) are very informative. They display uncoupled OD stretching modes of matrix isolated HDO and D_2O molecules. Hence each band observed in the spectra is due to a distinct hydrogen position in the structure. On one hand the peak frequency can be correlated with bond length and on the other hand the band width offers direct correlation with local bond geometry (angles). Splitting of degenerated or coupled or overlapped modes succeeds by high resolution measurements at low temperature.

At room temperature, the large peak around 1640 cm^{-1} in the α-Hopeite spectrum corresponds to the internal bending (ν_3) vibration of crystal water molecules while the broad, very strong band centered around 3300 cm^{-1} represents stretching (ν_1 and ν_3) modes, shifted to lower frequencies from their ideal value due to hydrogen bonding (Fig. 5). It is possible to determine the number of crystallographic non-equivalent type of water molecule from the frequency components at 3000–3600 cm^{-1} (asymmetrical and symmetrical valence vibrations of OH^- groups). While only two and three types of crystalline water can be identified within β- and α-Hopeite respectively at 25 °C, the increasing partial substitution (up to 75%) of water with D_2O at 90 K may indicate the existence of four non-energetically equivalent hydrogen bonds, i.e. two crystallographically different H_2O molecules in β-Hopeite (3519, 3450, 3374 and 3222 cm^{-1}) and six for α-Hopeite (3451, 3388, 3322, 3275, 3213, 3136 cm^{-1}). This complies very well with crystallographic data since among the three different crystal waters of α-Hopeite, two occupy a site of C_s symmetry and thus four uncoupled OD stretching modes are expected at least. In addition, bands at 3521, 631 and 352 are assigned to stretching modes (ν_S), libration mode (ν_L) and translational mode (ν_T) of the hydroxyl group alone [102, 103]. Therefore, HAP displays a broad shoulder in the region 3462–3033 cm^{-1} and near 3542 cm^{-1}, indicating a vertical oscillation of the hydroxyl groups along the crystallographic *c*-axis approaching and going away from the neighbouring plane defined by three calcium ions [104]. Such patterns do not exist for the Hopeite polymorphs. In consequence only one sharp peak at 3518 cm^{-1} is seen. The shapes of the H_2O stretching region of Brushite and HAP are significantly different from those of α- and β-Hopeite, with one band showing decoupling at 1647 and 1671 cm^{-1}, which indicates at least two types of water molecules [105] in the case of Brushite. In the DRIFT spectrum (Fig. 5), the presence of two separated narrow peaks at 1635 and 1584 cm^{-1} and the absence of marked peaks at 1435 cm^{-1} and 1465 cm^{-1} indicate either one type of well stabilized OH group in the HAP structure [106a] or the formation of Ca-deficient HAP thanks to the partial substitution of PO_4^{3-} with HPO_4^{2-} groups. The presence of a small but well defined peak at 1560 cm^{-1} excludes absolutely the incorporation of carbonates in the HAP structure [106b].

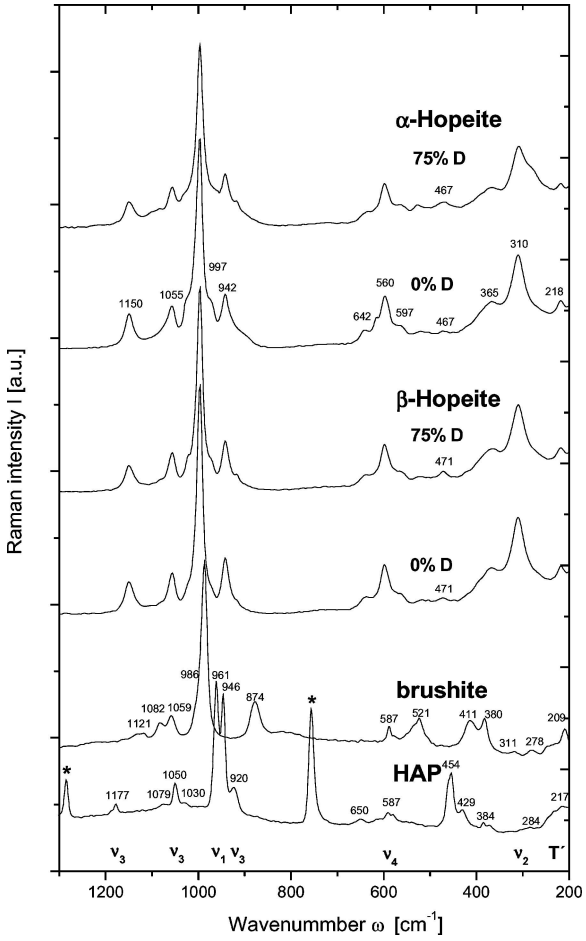

Figure 6 FT-Raman spectra of orthorhombic α- and β-$Zn_3(PO_4)_2 \cdot 4H_2O$ (α- and β-Hopeite) in the extended phosphate region 1300–200 cm^{-1}. Comparison with Brushite and Hydroxyapatite (HAP).

While α-,β-Hopeite show a broad shoulder in the range 623–575 cm^{-1}, Brushite exhibits one well defined peak at 658 cm^{-1} and HAP at 668 cm^{-1}, corresponding to OH libration ((H–O)–P=O) frequencies [73a].

The Raman spectra (Fig. 6) show a band at 310 cm^{-1} for the Hopeite polymorphs, at 311 cm^{-1} for Brushite and a weak band at 333 cm^{-1} for HAP, attributed to Zn–OH and Ca–OH bonds in each case. The latter one may indicate that the Ca–OH bond is partially covalent, in reference to Fowler's data on HAP (343 cm^{-1}) [104]. The 630 or 655 cm^{-1} bands (hydroxyl libration mode) appearing well separated from PO_4^{3-} vibration in the HAP Raman spectrum, is seen slightly shifted in the α-,β-Hopeite due to structure stabilization via hydrogen bonding. Distinction between α- and β-Hopeite succeeds by a weak band at 3207 cm^{-1} (α-form, 0%D), displaced to 3223 cm^{-1} with 75% hydrogen substitution for α-Hopeite, and to 3218 cm^{-1} for β-Hopeite. Similarly well identified peaks appear at 3082 cm^{-1} in the case of Brushite and at 3554 and 3225 cm^{-1} for HAP, attributed by Freund *et al.* to H_2O librations and a valence vibration [107].

TABLE III Distances of OD· · ·O hydrogen bonds in α- and β-Hopeite: Comparison between crystallographic data and correlations from averaged OD stretching modes $\nu_{OD}(cm^{-1})$ [DRIFT/FT-Raman] of matrix isolated HDO molecules in dilute samples (50%D). Measurement errors are for the lengths (DRIFT-XRD) are as follows: ±0.01 Å, ±0.01 Å

Hydrogen bonding				Distances (Å)					
Donor O_a (water)	H_i	Receptor O_b (PO_4)	ν_{OD} 298 °K (cm^{-1})	[a] O_a—O_b	[a] O_a—H	[a] H—O_b	[b] O_a—O_b	[c] O_a—H	[b] H—O_b
				α-Hopeite					
O (8)	H (8)	O (6)	3174	2.78	0.793	1.72	2.66	0.95	1.70
O (10)	H (10-1)	O (4)	3244	2.71	0.873	1.83	2.71	0.96	1.76
O (10)	H (10-2)	O (5)	3362	3.02	0.950	2.07	2.77	0.96	1.82
O (9)	H (9-1)	O (10)	3386	2.89	0.747	2.22	2.83	0.97	1.88
O (9)	H (9-2)	O (8)	3419	3.06	1.210	2.45	2.86	0.97	1.91
O (9)	H (9-2)	O (6)	3519	3.12	0.793	2.45	2.97	0.98	2.02
				β-Hopeite					
O (10)	H (10-1)	O (2)	3172	2.71	0.99	1.78	2.67	0.95	1.71
O (10)	H (10-2)	O (5)	3273	3.02	0.89	2.14	2.72	0.96	1.76
O (9)	H (9-2)	O (6)	3358	3.12	1.10	2.20	2.80	0.97	1.85
O (8)	H (8)	O (10)	3517	3.22	1.14	2.34	2.97	0.98	2.02

[a] X-ray single crystal analysis [51].
[b] Calculated from the wavenumbers of the uncoupled OD stretching modes by using the correlation developed by Mikenda.
[c] Calculated from the wavenumbers of the uncoupled OD stretching modes using LJ method.

A conclusive assignment of the uncoupled OD stretching modes of α- and β-Hopeite (Figs. 5 and 6) to their six and four crystallographically different hydrogen positions is shown in Table III. The assignement of the hydrogen bonds reported in [68] is mainly confirmed. The O-O, O-D and D· · ·O distances calculated from the wavenumbers of the uncoupled OD stretching modes as observed in FT-Raman and DRIFT spectra, by using the correlation curves of Lutz-Jung (LJ method) [108, 109] and Mikenda [110], are in good agreement with the crystallographic data [28], and they indicate strong hydrogen bonds.

Phosphate tetrahedra and structure stability

It is interesting to consider the spectral modifications related to the restructuring of phosphate anions in the conformational evolution from β-Hopeite to α-Hopeite. A lowering of tetrahedral symmetry (from T_d to C_1), due to the dynamic interactions of ions in the unit cell, caused by the formation of hydrogen bonds between the water molecules and PO_4^{3-} ions or the coordination via the Zn^{2+} cations, is observed by Raman spectroscopy since the ν_1 and ν_2 modes are prohibited in the IR spectrum by the selection rules. Further information can be gained by comparison with Brushite (presence of HPO_4^{2-}) and Hydroxyapatite (PO_4^{3-}-OH interactions).

Thus in Fig. 5, α- and β-Hopeite show very similar IR spectra below 1200 cm^{-1} (phosphate region), confirming the uniformity of the non-hydrogen framework. The observed bands at 1102–1068–1005, 945–928, 635–584, and 414 cm^{-1} (last band not shown in Fig. 5) are assigned to ν_{as} (P—O)(ν_3), ν_s(P-O)(ν_1), δ_{as} (OPO)(ν_4) and δ_s(OPO)(ν_2). In comparison to α-Hopeite (orthorhombic) the ν_1 mode of the HAP intermediary compound (Brushite) is stronger, sharper and shifted to 911 cm^{-1}, indicating a more open or distorted sphere of coordination of phosphate groups [111, 112]. Multiple ν_3 vibrations in the region between 1220 and 1123 cm^{-1}, and characteristic peaks at 2480, 1722, 868 and 875 cm^{-1} [113–117] indicate that the calcium hydrogen phosphate dihydrate (Brushite) belongs to a less ordered space group (monoclinic) [118].

In particular, in Fig. 6, well defined Raman bands can be observed close to the frequencies of the free PO_4^{3-} modes. The centers of the PO_4^{3-} internal bands are shifted to higher energy by 10–15 cm^{-1} (one ν_1 at 997 cm^{-1} and three ν_3 modes at 1150, 1055 and 942 cm^{-1}) as compared to the free PO_4^{3-} ion, suggesting strong crystal field effects in the α- and β-Hopeite [119–120]. In Table IV, the frequencies and widths of the Raman peaks of α-, β-Hopeite are collected as they were determined from high resolution scans of the Raman bands observed in the spectra displayed in Fig. 6. As for the ν_1 and ν_3 modes, β-Hopeite has broader peaks (20% for ν_1 and 30% on ν_3 in average) than α-Hopeite due to (1) the different strength of the various P—O bonds as shown from the decrease of the corresponding P—O distances, viz. 1.56/1.57 (P_3-O_2), 1.53/1.1.54 (P_3-O_4), 1.52/1.52 (P_3-O_5) and 1.51/1.52 Å [using the atom definition of Fig. 2], and (2) the different coupling with Zn-O stretching vibration to the adjacent metal oxygen polyhedra such as $ZnO_2(H_2O)_4$ in the case of α-Hopeite. Similarly, group theory predicts 42 Raman

TABLE IV Frequencies and widths (in cm^{-1}) of the peaks observed in the Raman spectra of α- Hopeite and β-Hopeite [a]

Lattice modes		Internal PO_4^{3-} modes							
		ν_1		ν_2		ν_3		ν_4	
ω	Γ	ω	Γ	ω	Γ	ω	Γ	ω	Γ
				α-Hopeite					
218^{sh}	22	997	20	365^{sh}	89	942	17	560	31
310^{b}	41			471^{w}	23	1055	21	597	35
				503^{w}	10	1150	21	642^{sh}	26
				519^{w}	26				
				β-Hopeite					
217^{sh}	26	996	16	366^{sh}	94	941	29.	562	31
309	50			471^{w}	18	1057	21	598	28
				502^{w}	9	1148	26	637^{sh}	38
				515^{w}	28				

[(a)]The full widths at half height have been determined from Lorentzian fits to the observed peaks. [(sh) = shoulder, (w) = weak].
[(b)]A broad band is observed in this frequency region.

TABLE V List of chemical shifts from ^{1}H NMR signals for zinc and calcium phosphate hydrates

Phosphate compounds	**^{1}H NMR signals** δ_{iso}(ppm)
$Ca_{10}(PO_4)_6(OH)_2$	1.5 (OH^-), 3.2 ($(CH_3)_4N^+$)
$CaHPO_4{\cdot}2\ H_2O$	5.0 (H_2O), 10.3 (acidic H)
$Zn_3(PO_4)_2{\cdot}4\ H_2O$	7.0 (acidic H)
α-$Zn_3(PO_4)_2{\cdot}4\ H_2O$	5.7 (H_2O)
β-$Zn_3(PO_4)_2{\cdot}4\ H_2O$	5.8 (H_2O)

modes originating from the ν_2 tetrahedron modes. As can be seen from Fig. 6 and Table V, in the frequency region 365–520 cm^{-1} where those modes occur, four broad peaks are detected at 365, 471, 503 and 519 cm^{-1}. Considering the high sensitivity of the ν_2 mode to O─P─O bond angle deformation, the large widths of the peaks observed in this region (see Table IV) suggests contribution from ν_2 internal modes very close in energy due to small disorder-induced angular distortions of the tetrahedra, and weak coupling between ν_2 modes of different tetrahedra. It is well known that the tetrahedron ν_2 modes are of purely bond-bending character, whereas the ν_4 modes contain also a small stretching component [121]. Taking into account that the relative bond angle variation in α-,β-Hopeite is about 5 to 10% while the relative variation of bond length is only 3%, the ν_2 modes of α-,β-Hopeite, whose energy is determined by interactions depending on the O─P─O angles, are expected to be more sensitive to small variations of the O─P─O angles than the ν_4-type mode for which the energy contains also a bond-stretching contribution. Therefore with 75%D substitution, the relative ratio {[ν_2 (75%D)/ν_1 (75%D)]/[ν_2(0%D)/ν_1(0%D)]} of the peak areas taken at 519 (515) and 997(996) cm^{-1} for the α-form and β-form respectively, is 1.47 and 3.48, and is a direct quantification of O-P-O angles fluctuations and bond flexibility.

Since Nuclear Magnetic Resonance (NMR) spectroscopy can be applied not exclusively for liquids but also for solids, it gives a complete view of the crystal structure and particularly of the phosphate chain geometry at a molecular level. In solids, broadening interactions of nuclear spins are no longer averaged; consequently the solid NMR spectra are characteristically broadened. In principle, the line width in amorphous and crystalline materials is related to the chemical environment and the local mobility with the sample investigated, and thus gives complementary information to FT-Raman and DRIFT spectroscopy. The lines width of ^{1}H and ^{31}P spectra in solid state NMR can be reduced by spinning the sample at the NMR magic angle (Magic Angle Spinning, MAS) where typical rotation frequencies are currently in the range of 5 to 35 kHz.

Fig. 7 depicts the ^{31}P MAS NMR spectra of various zinc and calcium phosphate hydrates. Despite their same chemical composition, it is possible to distinguish the α-Hopeite from the β-Hopeite, as they were found to resonate 4.52 ppm and 4.34 ppm in a single peak, indicating the presence of only one type of chemically

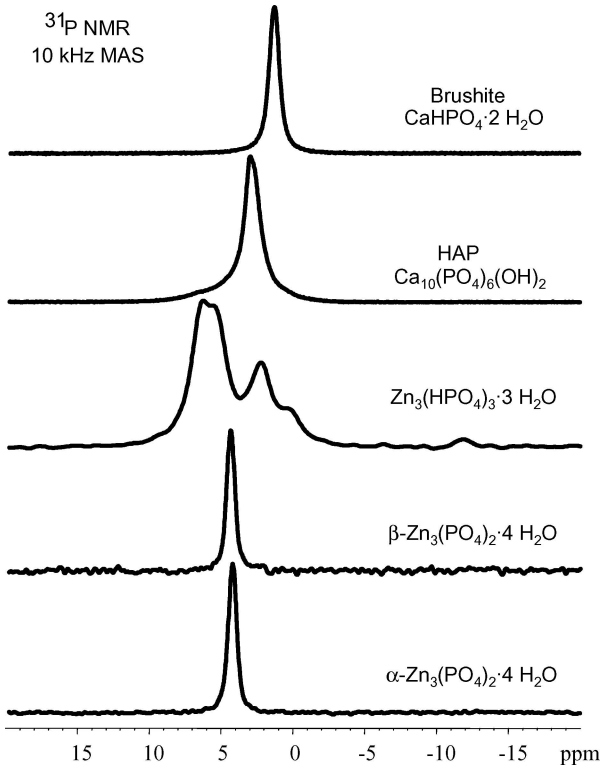

Figure 7 Slow spinning ^{31}P MAS NMR spectra of α-Hopeite and β-Hopeite, compared with $Zn_3(HPO_4)_3{\cdot}3H_2O$, Brushite and Hydroxyapatite. All ^{31}P NMR spectra were referenced with respect to 85% H_3PO_4 (0 ppm), with upfield shifts taken as negative. Note that liquid water is generally found to resonate at 4.7 ppm in a sharp resonance frequency.

equivalent phosphorus atom in both structures. Similarly, Sato mentioned a main chemical shift of 4.59 ppm for Hopeite coatings [122], which is in good agreement with the chemical shift δ [^{31}P] (namely σ_{iso}) of α-Hopeite. In addition, the ^{31}P MAS NMR spectra of Hopeite polymorphs show one isotropic resonance with a corresponding array of sidebands separated at a sample spinning speed of 10 kHz. While zinc hydrogen phosphate show multiple ^{31}P NMR signals (2.3, 5.5 and 6.5 ppm), Hydroxyapatite and particularly Brushite (calcium hydrogen phosphate) display broad singulets at 3.1 and 1.3 ppm respectively. Besides ^{31}P MAS NMR, a method sensitive to the chemical structural environment of phosphate, ^{1}H MAS NMR additionally monitors both inhomogeneities in the mobility of the components and between bulk components or adsorbed ones. While most components of α-Hopeite, distincts from the β-Hopeite, are quite rigid (crystal water) and contribute to broad resonances at 5.7 and 5.8 ppm, the β-form displays a second sharp resonance at 6.5 ppm, corresponding presumably to preferentially oriented hydrogen bonds (see Table V).

Concerning HAP, the peak at 1.5 ppm corresponds to the OH groups located in the HAP channels along the *c*-axis, and shifted from its known value of 0.2 ppm [123] due to the presence of TMA. Yesinowski and Eckert [124] observed at nearly the same position in the case of fluoroapatite and assigned it to hydroxyls in the neighbourhood of fluorine. The broad peak centered at 3.2 ppm is assigned to synthesis additive (tetramethylammonium hydroxide) and to adsorbed and/or structural water. The corresponding IR bands could be found at 3547 and 3541 cm^{-1} as shown in Fig. 5 [125]. Thus for zinc phosphate hydrate systems, ^{1}H MAS NMR spectroscopy can distinguish different ^{1}H chemical state more definitely, as compared with DRIFT or FT-Raman spectroscopy.

Conclusion

In conclusion, pure α- and β-Hopeite have been prepared in pure form by hydrothermal crystallization from aqueous solution at 20 °C and 90 °C. Their respective thermodynamic properties have been established and their interrelation has been confirmed by means of X-Ray diffraction method (XRD) at various temperatures, and thermal analysis (DSC) combined with TGA-MS. Using a heterogeneous step-reaction approach, the kinetics of dehydration of α- and β-HHopeite was studied. Metastable β-Hopeite was found to transform spontaneously in its more stable form, α-Hopeite around 168 °C. In synergy with these classical methods, powerful spectroscopic methods such as low temperature DRIFT, FT-Raman and ^{1}H, ^{31}P MAS-NMR were employed, revealing oriented distortions of the zinc phosphate tetrahedra, in accordance with the crystallographic hydrogen bond pattern and the molecular tetrahedral linkage scheme. Besides, biological Hydroxyapatite (HAP) and one of its precursors (Brushite) were also obtained and used to underline the resulting variations of surface chemical reactivity in zinc phosphates. The knowledge of the crystal structure, the particular thermal behaviour and the distortion of the phosphate groups in zinc phosphate tetrahydrates permits the understanding of the bulk properties. Further this may give insight to the complex surface reactivity of such biomaterials.

Acknowledgments

The authors thank the Bundesministerium für Bildung und Forschung-German Education & Reseach Ministry (BMBF) for financial support of this work under the project "Water as medium for synthesis, transformations and applications of plastics" and also BASF AG. Special thanks are extended to Dr. Castignolles for the helpful discussions.

References

1. P. M. BILLS and E. J. WHEELER, *J. Ed. Mod. Mater. Sci. Eng.* **4** (1982) 391.
2. A. SCHUROVSKY, Y. YACKIEVYCH and A. SHYYKA, *Bone* **32**(5) (2003) S105.
3. L. L. HENCH and J. WILSON, in "Advances Series in Ceramics", (World Scientific Publishers, Singapore, 1993) Vol. 1.
4. L. J. SHYU, L. PEREZ, S. ZAWACKI, J. C. HEUGHEBAERT and G. H. NANCOLLAS, *J. Dent. Res.* **62** (1983) 398.
5. W. E. BROWN and L. C. CHOW, in Cement Research Progress, edited by P. W. Brown, (Am. Ceramics. Soc., Westerville, OH, 1987), p. 351.
6. B. R. CONSTANZ, I. C. ISON, M. T. FULMER, R. D. POSER, S. T. SMITH, M. VANWAGONER, J. ROSS, S. A. GOLDSTEIN, B. J. JUPITER and D. I. ROSENTHAL, *Science* **267** (1995) 1796.
7. L. L. HENCH, *J. Am. Ceram. Soc.* **74** (1991) 1487.
8. E. F. MORGAN, D. N. YETKINLER, B. R. CONSTANZ and R. H. RAUSKARDT, *J. Mater. Sci.: Mater. Med.* **8**(9) (1997) 559.
9. G. GOLLER and F. N. OKTAR, *Mater. Lett.* **56**(3) (2002) 142.
10. A. GERLACH, B. VINCENT, M. LISSAC, X. ESNOUF and G. THOLLET, *Biomater.* **14** (1993) 770 and references therein.
11. F. BOHLSEN and M. KERN, *Quintessence Int.* **34**(7) (2003) 493.
12. N. HIRAISHI, Y. KITASAKO, T. NIKAIDOL, R. M. FOXTON, J. TAGAMI and S. NOMURA, *Int. Endod. J.* **36**(9) (2003) 622.
13. B. CZARNECKA, H. LIMANOWSKA-SHAW and J. W. NICHOLSON, *J. Mater. Sci.: Mater. Med.* **14**(7) (2003) 601.
14. J. W. NICHOLSON, B. CZARNECKA and H. LIMANOWSKA-SHAW, *ibid.* **10**(8) (1999) 449.
15. A. D. WILSON, B. E. KENT and B. G. LEWIS, *J. Dent. Res.* **49** (1970) 1049.
16. S. CRISP, I. K. O'NEILL, H. J. PROSSER, B. STUART and A. D. WILSON, *ibid.* **57** (1978) 254.
17. J. MARGERIT, B. CLUZET, J. M. LEHOUP, J. NURIT, B. PAUVERT and A. TEROL, *J. Mater. Sci. Mater. Med.* **9** (1999) 449.

18. J. O. NRIAGU, *Geochim. & Cosmochim. Acta* **37** (1973) 2357.
19. M. UO, G. SJOREN, A. SUNDH, *et al.*, *Dent. Mater.* **19**(6) (2003) 487.
20. N. ATTAR, L. E. TAM and D. MCCOMB, *J. Prothet. Dent.* **89**(2) (2003) 127.
21. N. J. A. GREY and J. F. MCCORD, *J. Dent. Res.* **80**(4) (2001) 1152.
22. R. J. HILL and J. B. JONES, *Am. Mineralogist* **61**(9-10) (1975) 987.
23. G. Y. CHAO, *Z. Kristallogr.* **130** (1969) 261.
24. M. V. GOLOSHCHAPOV and T. N. FILATOVA , *Russ. J. Inorg. Chem.* **14**(3) (1969) 424.
25. E. A. NIKONENKO and I. N. MARENKOVA, *ibid.* **31** (1986) 397.
26. H. M. A. AL-MAYDAMA and P. J. GARDNER, *Electrochem. Acta* **194** (1992) 117.
27. H. M. A. AL-MAYDAMA, P. J. GARDNER and I. W. MC ARA, *ibid.* **196** (1992) 117.
28. L. HERSCHKE, V. ENKELMANN, I. LIEBERWIRTH and G. WEGNER, *Chem. Eur. J.* **10**(11) (2004) 2795.
29. N. SATO, K. WATANABE and T. MINAMI, *J. Mater. Sci* **26**(4) (1991) 865.
30. S. HAUSSUHL and M. FRIEDRICH, *Cryst. Res. Technol.* **28**(4) (1993) 437.
31. P. LUO, in "Methods for Synthesizing HA Powders and Bulk Materials", US Patent: 5858318 (1996).
32. C. C. BERNDT, G. N. HADDAD, A. J. D. FARMER and K. A. GROSS, *Mater. Forum* **14**(3) (1990) 161.
33. M. AKAO, H. AOKI and K. KATO, *J. Mater. Sci.* **6** (1981) 809.
34. M. V. CABANAS and M. VALLET-REGI, *J. Mater. Chem.* **13**(5) (2003) 1104.
35. J. L. ARIAS, M. B. MAYOR and J. POU, *Appl. Surf. Sci* **208** (2003) 57.
36. O. PAWLING and R. TRETTIN, *Mat. Res. Bull.* **34**(12-13) (1999) 1959.
37. S. V. DOROZHKIN and M. EPPLE, *Angew. Chem. Int. Edit.* **41**(17) (2002) 3130.
38. E. LANDI, G. CELOTTI, G. LOGROSCINO and A. TEMPERI, *J. Eur. Ceram. Soc.* **23**(15) (2003) 2931.
39. R. A. YOUNG, in Proceedings of the 2nd International Congress on Phosphorous Compounds, (Inst. Mond. Phosp., Paris, 1980), p. 73.
40. L. M. RODRIGUEZ-LORENZO, J. N. HART and K. A. GROSS, *Biomater.* **24**(21) (2003) 3777.
41. E. I. DOROZHKINA and S. V. DOROZHKIN, *Colloid & Surface* A **210**(1) (2002) 41.
42. W. E. BROWN, *Nature* **196** (1962) 1048.
43. B. HERMANN, *Z. Morphol. Anthropol.* **68** (1977) 129.
44. G. LUSVARDI, L. MENABUE and M. SALADINI, *J. Mater. Sci.: Mater. Med.* **13**(1) (2002) 91.
45. P. BODIER-HOULLÉ, *J. Dent. Res.* **76** (1997) 895–904.
46. A. D. WILSON, G. ABEL and B. G. LEWIS, *Br. Dent. J.* **137** (1974) 313.
47. R. A. BARREA, C. A. PEREZ and A. Y. RAMOS, *X-Ray Spectrom.* **32**(5) (2003) 387.
48. S. V. DOROZHKIN, *Prog. Cryst. Growth* **44**/1 (2002) 45.
49. J. LANG, *Bull. Soc. Chem. Bret.* **53** (1981) 95.
50. C. ROLLAND, R. GUIDOIN, R. LEDOUX, A. ZERGUINI and P. E. ROY, *Can. Mineral.* **29** (1991) 337.
51. J. TERRA, M. JIANG and D. E. ELLIS, *Philos. Mag.* A **82**(11) (2002) 2357.
52. S. KENNY, M. BUGGY and R. G. HILL, *J. Mater. Sci.: Mater. Med.* **12**(10-12) (2001) 901.
53. R. Z. LEGEROS, C. B. BLEIWAS, M. RETINO, R. ROHANIZADEH and J. P. LEGEROS, *Am. J. Dent.* **12**(2) (1999) 65.
54. M. KNUUTTILA, R. LAPPALEÁINEN and V. KONTTURI-NARHI, *Scand. J. Dent. Res.* **88** (1980) 513.
55. A. BIGI, E. FOREST, M. GANDOLFI, M. GAZZANO and N. ROOVERI, *J. Inorg. Biochem.* **66** (1997) 259.
56. S. C. D'ANDREA and A. Y. FADEEV, *Langmuir* **19**(19) (2003) 7904.
57. R.R. ERNST, G. BODENHAUSEN and A. WOKAUN, "Principles of Nuclear Magnetic Resonance in One and Two Dimensions", (Clarendon Press, Oxford, 1986).
58. O. G. GORENSTEIN, "Phosphorus-31 NMR – Principles and applications", (Academic press, Orlando, 1984).
59. A. L. VOLKOV, V. N. YAGLOV and G. L. NOVIKOV, *Russian J. Phys. Chem.* A**48** (1974) 1697.
60. V. N. YAGLOV, *Khim. Khim. Tekhnol.* (Minsk) **13** (1978) 7.
61. J. S. STEPHENS and C. CALVO, *Can. J. Chem.* **45** (1967) 2303.
62. Y. CUDENNEC, A. LECERF, A. RIOU and Y. GÉRAULT, *C. R. Acad. Sci.* **301** serie II (1985) 93.
63. J. KOMRSKA and V. SATAVA, *Silikaty* **13**(2) (1969) 135.
64. F. L. KATNACH and F. A. HUMMEL, *J. Electrochem. Soc.* **105** (1958) 125.
65. ICDS cards of α,β-$Zn_3(PO_4)_2$ N° 29–1390 and 30–1489.
66. A. G. KOTLOVA, N. I. SHCHEEPOCHKINA and B. M. KOBSEV, *Inorg. Mater.* (USSR) **11** (1976) 1247.
67. Y. ARNAUD, E. SAHAKIAN and M. ROMAND, *Appl. Surf. Sci.* **32** (1988) 281.
68. A. WHITAKER, *J. Appl. Cryst.* **6** (1973) 495.
69. T. KANAZAWA, in Inorganic Phosphate Chemistry, edited by Kodansha Scientific, (Tokyo, 1985).
70. Y. ARNAUD, E. SAHAKIAN, J. LENOIR and A. ROCHE, *Appl. Surf. Sci.* **32** (1988) 296.
71. H. HAIDARA, PhD. Thesis, University of Muhlhouse, (France), (1985).
72. E. A. NIKONENKO, I. I. OLIKOV, I. N. MARENKOVA, L. N. MARGOLIN and L. A. REZNIKOVA, *Russ. J. Inorg. Chem.* **30** (1985) 25.
73. (a) V. S. JOSHI and M. J. JOSHI, *Cryst. Res. Technol.* **38**(9) (2003) 817; (b) N. JINLONG, Z. ZHENXI and J. DAZONG, *J. Mater. Syn. Proc.* **9**(5) (2002) 235; (c) J. T. DICKINSON, C. BANDIS and S. C. LANGFORD, *Mat. Res. Soc. Symp.* **617** (2000) J1.1.1
74. (a) C. CAMERON and B. BEN-NISSAN, *Int. Ceram. Monographs*, **1**(1) (1994) 79; (b) W. Kubota, *Nippon Seikeigeka Gakkai Zasshi* **66**(1) (1992) 110.
75. A. I. VOLKOV, V. N. YAGLOV and G. I. NOVIKOV, *Russ. J. Phys. Chem.* **48** (1974) 1697.
76. *Idem.*, *ibid.* **48** (1974) 1701.
77. V. N. YAGLOV, *Khim. Khim. Technol.* (Minsk) **13** (1978) 7.
78. V. N. YAGLOV, L. A. MARINOVA and G. I. NOVIKOV, *Dokl. Akad. Nauk.* B**78** (1974) 624.
79. D. D. WAGMAN, W. H. EVANS, V. B. PARKER, I. HALOW, S. M. BAILEY and R. H SCHUMM, *Natl. Bur. Stand. Tech. Note* **270**(3) (1968) 264.
80. D. D. WAGMAN, W. H. EVANS, V. B. PARKER, I. HALOW, S. M. BAILEY and R. H SCHUMM, *Natl. Bur. Stand. Tech. Note* **270**(4) (1969) 152.
81. D. D. WAGMAN, W. H. EVANS, V. B. PARKER, I. HALOW, S. M. BAILEY, R. H SCHUMM and K. L. CHURNEY, *Natl. Bur. Stand. Tech. Note* **270**(5) (1971) 49.
82. I. R. GIBSON, I. REHMAN, S. M. BEST and W. BONFIELD, *J. Mater. Sci.: Mater. Med.* **12** (2000) 799.
83. M. TAMAI, M. NAKAMURA, T. ISSHIKI, H. ENDOH and A. NAKAHIRA, *J. Mater. Sci. Mater. Med.* **14** (2003) 617.
84. J. JP. VALDES, J. O. LOPEZ, G. R. MORALES, G. P. MALAGON and V. P. GORTCHEVA, *J. Mater. Sci.: Mater. Med.* **5** (1997) 297.

85. V. B. PARKER, D. D. WAGMAN, W. H. EWANS, *Natl. Bur. Stand. Tech. Note* **270**(6) (1971) 119.
86. J. D. COX, D. D. WAGMAN, V. A. MEDVEDEV, in CODATA Key Values for Thermodynamics, (Hemisphere Pub. Corp., London, 1989).
87. A. I. VOLKOV, *Khim. Khim. Tekhnol*. (Minsk) **14** (1979) 58.
88. V. N. YAGLOV, *ibid.* (Minsk) **13** (1978) 7.
89. J. O. NRIAGU and P. B. MOORE, in, "Phosphate Minerals", (Springer Verlag, Berlin, 1984).
90. F. BAITALOW, G. WOLF and H. G. SCHMIDT, *J. Thermal Anal.* **52** (1998) 5.
91. C. H. P. LUPIS, in "Chemical Thermodynamics of Materials", (Elsevier Publish., Oxford, 1983), p. 87.
92. R. S BERRY, S. A. RICE and J. ROSS, in "Physical Chemistry", (J. Wiley and Sons, 1980), p. 1147.
93. P. MOLERA, J. MONTOYA and M. DEL VALLE, *Corr. Rev.* **21**(4) (2003) 349.
94. A. BEHENCOURT, F. J. BOTANA, M. MARCOS, *et al*., *Prog. Org. Coat*. **46**(4) (2003) 280.
95. M. BEIRO, A. COLLAZO, M. IZQUIERDO, X. R. NÓVOA and C. PÉREZ, *Prog. Org. Coat*. **46**(2) (2003) 97.
96. U. B. NAIR and M. SUBBAIYAN, *J. Mater. Sci*. **30** (1995) 2108.
97. T. SUGAMA and T. TAKAHASHI, *ibid.* **30** (1995) 809.
98. O. PAWLIG, V. SCHELLENBERGER, H. D. LUTZ and R. TRETTIN, *Spectrochim. Acta* A**57** (2001) 581.
99. K. NAKAMOTO in "IR and Raman Spectra of Inorganic and Coordination Compounds", (J. Wiley & Sons, New York, 1986).
100. N. SATO, K. WATANABE and T. MINAMI, *J. Mater. Sci.* **26** (1991) 1383.
101. H. D. LUTZ, *Struct. Bonding* **82** (1988) 97.
102. J. ARENDS, J. CHRISTOFFERSEN, M. R. CHRISTOFFERSEN, H. ECKERT, *et al*., *J. Cryst. Growth* **84** (1987) 512.
103. J. J. STUTTMANN, J. D. TERMINE and A. S. POSNER, *Trans. NY Acad. Sci*. **27** (1965) 669.
104. B. O. FOWLER, *Inorg. Chem*. **13** (1974) 194.
105. O. PAWLIG and R. TRETTIN, *Chem. Mater.* **12** (2000) 1279.
106. (a) B. O. FOWLER, E. C. MORENO and W. E. BROWN, *Arch. Oral. Biol.* **11** (1966) 477; (b) M. PRETTO, A. L. COSTA, E. LANDI, A. TAMPIERI, *et al*., *J. Am. Ceram. Soc.* **86**(9) (2003) 1534.
107. F. FREUND and R. M. KNOBEL, *J. Chem. Soc*. **6** (1977) 1136.
108. H. D. LUTZ, *Struct. Bonding* (Berlin) **82** (1995) 85.
109. H. D. LUTZ and C. JUNG, *J. Mol. Struct*. **404** (1997) 63.
110. W. MIKENDA, *ibid.* **147** (1986) 1.
111. H. D. LUTZ, J. HIMMRICH and M. SCHMIDT, *J. Alloys Compd*. **241** (1996) 1.
112. V. PERUSEVSKI and B. SOPTRAJANOV, *J. Mol. Struct.* **17** (1988) 349.
113. E. E. BERRY and C. B. BADDIEL, *Spectrochim. Acta* A**23** (1967) 537.
114. A. C. CHAPMAN, D. A. LONG and D. L. JONES, *Spectrochim. Acta* A**21** (1965) 633.
115. J. A. S. BETT, L. G. CHRISTNER and W. KEITH HALL, *J. Am. Chem. Soc*. **89** (1967) 5535.
116. G. SOCRATES, in "Infrared Characteristic Group Frequencies", (J. Wiley & Sons, Chichester, 1980).
117. A. Y. U. MALYSHEVA and B. I. BELETSKII, *Glass and Ceram*. **58**(3) (2001) 147.
118. A. HINA, G. H. NANCOLLAS and M. GRYNPAS, *J. Cryst. Growth* **223** (2001) 213.
119. H. D. LUTZ and H. HAEUSELER, *Trends Appl. Spectrosc*. **2** (1998) 59.
120. *Idem*., *J. mol. Struct*. **511**(512) (1999) 69.
121. G. HERZBERG in Molecular Spectra and Molecular Structure II: Infra-Red & Raman Spectra of Polyatomic Molecules, edited by D. Van Nostrand, (Princeton, 1945).
122. N. SATO, *J. Mater. Sci. Lett*. **10**(2) (1991) 115.
123. T. ISOBE, S. NAKAMURA, R. NEMOTO and M. SENNA, *J. Phys. Chem*. B**106** (2002) 5169.
124. J. P. YESINOWSKI and H. ECKERT, *J. Am. Chem. Soc.* **109** (1987) 6274.
125. A. BAUMER, M. GANTEAUME and W. E. KLEE, *Bull. Mineral.* **108** (1985) 145.

Received 7 April 2004
and accepted 9 May 2005